INDERSCIENCE PUBLISHERS
Linking academia, business and industry through research


**International Journal of Vehicle Design**

ISSN online: 1741-5314 - ISSN print: 0143-3369
https://www.inderscience.com/ijvd

# Coupled electrothermal model and thermal fault diagnosis method for lithium-ion battery

Qiuting Wang, Wei Qi

**DOI:** 10.1504/IJVD.2024.10061813

**Article History:**

| | |
|---|---|
| Received: | 04 September 2021 |
| Accepted: | 18 May 2022 |
| Published online: | 23 January 2024 |

# Coupled electrothermal model and thermal fault diagnosis method for lithium-ion battery

Qiuting Wang* and Wei Qi

Department of Electrical and Information Engineering,
Hangzhou City University,
51 Huzhou Road, Hangzhou, 310015, China
Email: wangqt@hzcu.edu.cn
Email: qiw@hzcu.edu.cn
*Corresponding author

**Abstract:** The dynamic behaviour of lithium-ion battery system is analysed. The nonlinear parameters, residual errors and thermal faults of battery model are studied. In our study, a coupled electrothermal model is established based on the cell electrical dynamic characteristics. The parameter identification algorithm is presented based on Lyapunov observer. The core temperature and surface temperature of battery cell are calculated based on extended Kalman filter (EKF). We propose new thermal fault diagnosis method and the residual generation scheme. The urban dynamometer driving schedule (UDDS) dynamic working condition is used to verify our electrothermal model and fault diagnosis method. The experimental results indicate that the thermal characteristics can be described and the thermal fault can be diagnosed more accurately.

**Keywords:** lithium-ion battery; coupled electrothermal model; fault diagnosis; Lyapunov observer; EKF; extended Kalman filter; UDDS; urban dynamometer driving schedule.

**Reference** to this paper should be made as follows: Wang, Q. and Qi, W. (2024) 'Coupled electrothermal model and thermal fault diagnosis method for lithium-ion battery', *Int. J. Vehicle Design*, Vol. 94, Nos. 1/2, pp.83–99.

**Biographical notes:** Qiuting Wang received her Master and PhD degrees from Huazhong University of Science and Technology, Wuhan, China. Currently, she is a Teacher at the Department of Electrical and Information Engineering, Hangzhou City University. Her research interests include digital signal processing, lithium battery management system and Kalman filtering algorithm.

Wei Qi received his Master's and PhD degrees from Zhejiang University, Hangzhou, China. Currently, he is a Teacher at the Department of Electrical and Information Engineering, Hangzhou City University. His research interest is electronic circuits.

## 1 Introduction

Many researchers in and abroad have studied the safety, efficiency and stability of energy storage system for lithium-ion battery (Stoppanin, 2017). The research priorities include electrode material and structure design, behaviour description, status monitoring, fault detection and balancing control (Lian et al., 2020; Lam et al., 2018). An accurate thermal model is mainly needed describe the thermal accumulation, thermal convection and thermal conduction during battery working period (Li et al., 2017; Fan et al., 2018; Zou et al., 2018; Liu et al., 2019; Dong et al., 2018). Wang gave a detailed review of thermal model and thermal generation characteristic for lithium-ion battery (Wang et al., 2016; Mangoni and Soldati, 2021). The battery thermal model can be divided into two types: the Distributed Parameter model and the Lumped Parameter model. The battery thermal dynamic behaviour is described using a set of partial differential equations based on the distributed parameter model. The mechanisms of thermal accumulation, thermal convection and thermal conduction are defined using differential equations. The battery cell is considered as a whole part based on the Lumped Parameter model. Yang proposed an equivalent thermal model and the thermal dynamic behaviour is simulated using equivalent circuit elements (Yang et al., 2019). Fang presented a thermal concentration parameter model using one dimensional (1D) electrochemical model (Fang et al., 2010). Biron further proposed a second-order state equation based on the thermal parameters defined as core temperature and surface temperature.

The battery system safety is critically related to the electrochemical characteristics, the thermal performance and the ageing state (Chaou and Ibe-Ekeocha, 2017). The factors are coupled and interact with each other. The ageing state and the thermal performance is related to the total available capacity, internal resistance and other parameters. The battery current, terminal voltage and open circuit voltage (OCV) will conversely affect the thermal performance. The battery models and thermal models presented recently can simulate the battery electrochemical characteristics and the thermal behaviour. However, they are considered independent to each other (Zhang et al., 2019). The electrical models presented in Chen et al. (2019) are depended on the estimation value of battery capacity and resistance. Both are related to the environment temperature, ageing state and other factors. It undoubtedly limits the robustness of the battery model and the parameter identification process (Liu and He, 2017). Therefore, it is necessary to establish the coupled electrothermal model to simulate the battery dynamic behaviour accurately.

The rest of the paper is as follows: Section 2 introduces the thermal generation mechanism of lithium-ion battery. The coupled electrothermal model and parameter identification process based on Lyapunov observer are presented in Section 3. In Section 4, the state estimation algorithm based on extended Kalman filter(EKF) is put forward. The thermal fault diagnosis method is established in Section 5 and the experimental results are analysed in Section 6.

## 2 Thermal generation mechanism

Practically, the electrical parameters and thermal parameters of lithium-ion battery model are difficult to be measured directly. Based on (Yassine and Anderson, 2020), the temperature distribution of cylinder cell is described as follows,

$$\begin{aligned}\rho^j c^j \frac{\partial T^j(x,t)}{\partial t} &= \lambda^j \frac{\partial^2 T^j(x,t)}{\partial x^2} - (I(t) - i_e^j(x,t)) \frac{\partial \Phi_s^j(x,t)}{\partial x} \\ &\quad - i_e^j(x,t) \frac{\partial \Phi_e^j(x,t)}{\partial x} + Fs^j J^j(x,t) \eta^j(x,t) \\ &\quad + Fs^j J^j(x,t) T^j(x,t) \Delta_s^j\end{aligned} \tag{1}$$

where, $j$ indicates the positive pole, negative pole and the diaphragm. It is defined as $j \in \{+,-,sep\}$. $\rho$ is the mass density of the battery, $c$ is the specific heat, $T$ is the battery temperature, $\lambda$ is the thermal conductivity, $I$ is the load current. $i_e(x,t)$ represents the local current of electrolyte. $\Phi_s$ and $\Phi_e$ are the electrode potential and electrolyte potential, respectively. $F$ is the Faraday constant, $s$ is the cross-sectional area of solid particle surface, $J$ is the total ion flux on solid particle surface. $\Delta_s$ indicates the entropy change.

The dynamic change of battery temperature is directly related to the electrical variables defined as $\Phi_s$, $\Phi_e$ and $i_e$. However, the temperature distribution model is satisfied the partial differential equation. The cell radial thermal production is assumed unified in our study. Therefore, the thermal dynamic equation can be simplified as follows (Richardson et al., 2018),

$$\rho c_p \frac{\partial T(r,t)}{\partial t} = \lambda \frac{\partial^2 T(r,t)}{\partial r^2} + \frac{\lambda}{r} \frac{\partial T(r,t)}{\partial r} + \frac{Q(t)}{V_b} \tag{2}$$

where, $c_p$ is the specific thermal capacity, $V_b$ is the cell volume, $Q(t)$ is the thermal production, $r$ is the radial length, $t$ is the sample time. According to the dynamic change of battery temperature distribution, the boundary conditions are shown as equations (3) and (4),

$$\frac{\partial T(r,t)}{\partial r}\Big|_{r=0} = 0 \tag{3}$$

$$\frac{\partial T(r,t)}{\partial r}\Big|_{r=R} = \frac{h}{\lambda}(T_s - T_e) \tag{4}$$

where, $R$ only defines the cell radius. $T_s$ and $T_e$ are the surface temperature and environment temperature, respectively. $h$ is the convection coefficient. The distributed parameter model shown in equation (2) is not suitable for online working condition. The computing procedure is complex and the parameter identification is difficult. A Lumped Parameter model is designed to describe the dynamic characteristics. The core temperature defined as $T_c$ and the surface temperature $T_s$ are the model state vectors. The input vector is thermal production and the output vector is $T_s$. The state space equation can be expressed as follows:

$$a_c \dot{T}_c = \frac{T_s - T_c}{R_c} + Q_{gen} \tag{5}$$

$$a_s \dot{T}_s = -\frac{T_s - T_c}{R_c} + \frac{T_e - T_s}{R_u} \tag{6}$$

where, $a_c$ and $a_s$ are the heat capacity coefficients of the inside materials and battery surface, respectively. $R_c$ is the thermal resistance between battery core and battery surface. $R_u$ is the convection resistance between battery surface and surrounding environment. $Q_{gen}$ is the thermal production rate and it can be expressed as follows,

$$Q_{gen} = I_L(U_t - U_{oc}) + I_L T \frac{\partial U_{oc}}{\partial T} \tag{7}$$

where, $I_L$ is the load current, $U_t$ and $U_{oc}$ are battery terminal voltage and OCV, respectively. The thermal value in equation (7) is caused by Ohmic loss and charge transfer overvoltage. The energy dissipated by electrode overvoltage is ignored to simplify our research (Richardson et al., 2017).

## 3 Coupled electrothermal model and parameter identification algorithm

### *3.1 Dynamic electrical model*

To simplify the main problems, the one-order RC equivalent circuit model is established as shown in Figure 1. $R_o$ is the Ohmic resistance, $R_1$ and $C_1$ are the equivalent polarisation resistance and capacity, respectively. $U_{oc}$ is the OCV, $U_t$ is the terminal voltage.

**Figure 1** One-order RC equivalent circuit model

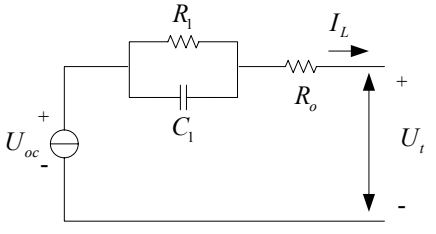


According to Kirchhoff's law and Ohm's law, the dynamic behaviour of the equivalent circuit model can be expressed as follows (Wu et al., 2017),

$$\dot{U}_1 = -U_1/(R_1C_1) + I_L/C_1$$
$$U_t = U_{oc} - I_L R_o - U_1 \tag{8}$$

where, $U_1$ is the cross voltage of $R_1C_1$ parallel circuit. The function term $I_L R_o$ describes the voltage transient caused by Ohmic resistance. Function (8) can be discretised as follows,

$$U_{1,k+1} = \exp\left(-\frac{\Delta t}{R_1 C_1}\right) U_{1,k} + \left(1 - \exp\left(-\frac{\Delta t}{R_1 C_1}\right)\right) R_1 I_{L,k} \tag{9}$$

$$U_{t,k} = U_{oc,k} - U_{1,k} - I_{L,k} R_o \tag{10}$$

where, $\Delta t$ is the sampling time. Our previous experimental results indicate that the relationship of OCV and SOC is basically stable during the battery ageing process. However, the OCV is the time-varying parameter and it changes slowly. The value can be described as $\dot{U}_{oc} \approx 0$. Rewrite the function (8) by bring the parameter $U_1$ as function (11),

$$\begin{aligned} \dot{U}_t &= \dot{U}_{oc} - \dot{I}_L R_o - \dot{U}_1 \\ &= \dot{U}_{oc} - \dot{I}_L R_o + \frac{U_1}{\tau} - \frac{I_L}{C_1} \\ &= \dot{U}_{oc} - \dot{I}_L R_o + \frac{U_{oc} - I_L R_o - U_t}{\tau} - \frac{I_L}{C_1} \\ &= -\frac{U_t}{\tau} + \dot{U}_{oc} + \frac{U_{oc}}{\tau} - \frac{R_{dc} I_L}{\tau} - R_o \dot{I}_L \end{aligned} \tag{11}$$

where, $\tau$ and $R_{dc}$ are defined as $\tau = R_1 C_1$ and $R_{dc} = R_o + R_1$, respectively. During the capacity attenuation and internal resistance increasing, the dynamic behaviour characteristics will change. The DC internal resistance $R_{dc}$ and capacity value must be updated online. Rewrite equation (11) as the state space equations (12)–(14),

$$\begin{cases} \left[\dot{U}_t\right] = \overbrace{\left[\frac{-1}{R_1 C_1}\right]}^{A} \overbrace{\left[U_t\right]}^{x} + \overbrace{\left[\frac{-I_L}{R_1 C_1} \quad \frac{-1}{R_1 C_1} \quad -\dot{I}_L\right]}^{f(x,u)} \overbrace{\begin{bmatrix} R_1 + R_o \\ U_{oc} \\ R_o \end{bmatrix}}^{\theta} \\ \underbrace{U_t}_{y} = \underbrace{[1]}_{C} \underbrace{[U_t]}_{x} \end{cases} \tag{12}$$

$$\begin{cases} \dot{x} = Hx + f(x,u)\theta \\ y = Cx \end{cases} \tag{13}$$

$$\begin{cases} \dot{\theta} = 0 \\ \dot{U}_t = HU_t + f(U_t, I_t)\theta \end{cases} \tag{14}$$

where, $x = [U_t]$ is the state vector, $H$ is the state transition matrix, $u = [I_L]$ is the battery input, $y$ is the battery output, $f(x,u)$ is the non-linear function. $C$ is the battery observation matrix. $\theta$ defines the electrical parameters and it satisfied as $\theta \triangleq [R_{dc}, U_{oc}, R_o]^T$. Other parameters are defined as follows,

$$f(U_t, I_L) \triangleq \left[\frac{-I_L}{\tau}, \frac{1}{\tau}, -\dot{I}_L\right]$$

$$H = \left[\frac{-1}{\tau}\right] \tag{15}$$

### 3.2 Coupled electrothermal model

The block diagram of coupled electrothermal model is shown in Figure 2. It includes three sub-models defined as equivalent circuit model, thermogenesis model and thermal model. The input and output vectors of the electrical model are the current $I_t$ and the terminal voltage $U_t$, respectively. The inputs of the thermal model are the environment temperature $T_e$ and thermal production rate $Q_{gen}$. The outputs of the thermal model are the core temperature $T_c$ and surface temperature $T_s$. As shown in Figure 2, the parameter $Q_{gen}$ depends on the value of OCV and the internal resistance.

**Figure 2** Block diagram of coupled electrothermal model (see online version for colours)

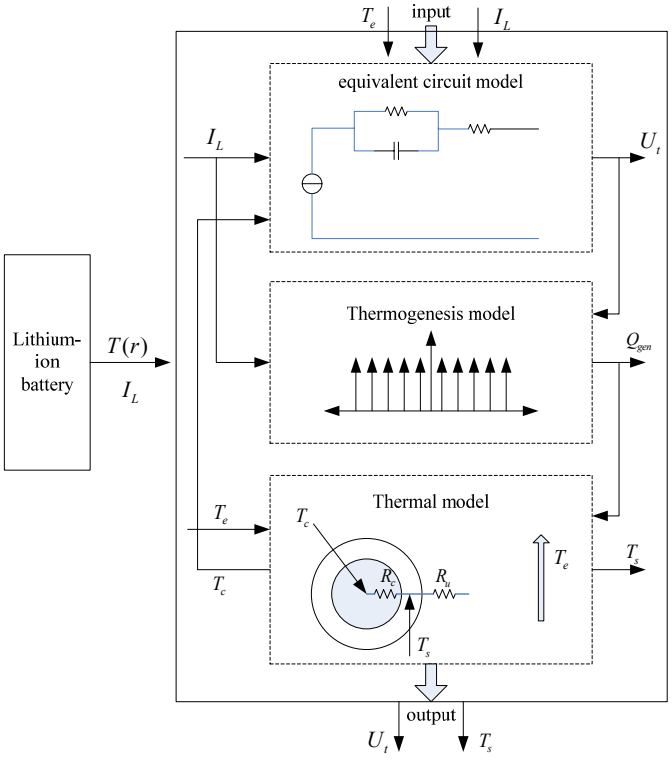


### 3.3 Parameter identification algorithm

The input vectors of equation (16) are $Q_{gen}$ and $T_e$. The output vector is $T_s$. The state vector is defined as $z = [T_c, T_s]^T$. The state space model can be discretised as follows,

$$z_{k+1} = A_d z_k + B_d u_{q,k} + \eta_k \tag{16}$$

$$y_{q,k} = \begin{pmatrix} g(z_{1,k}) \\ z_{2,k} \end{pmatrix} + v_k \tag{17}$$

where, $\eta_k$ and $v_k$ are the independent Gaussian noise. $u_q$ $u_q = \left[ Q_{gen}, T_e \right]^T$ and $y_q$ is defined as $y_q = \left[ \hat{R}_{dc}, T_s \right]^T$. $\hat{R}_{dc}$ is the estimated value of DC resistance. Considering function (5) and (6), the coefficient matrix $A_d$ and $B_d$ are as follows,

$$A_d = \begin{bmatrix} 1 - \dfrac{\Delta t}{R_c a_c} & \dfrac{\Delta t}{R_c a_c} \\ \dfrac{\Delta t}{R_c a_s} & 1 - \dfrac{\Delta t}{R_c a_s} - \dfrac{\Delta t}{R_u a_s} \end{bmatrix} \tag{18}$$

$$B_d = \begin{bmatrix} \dfrac{\Delta t}{a_c} & 0 \\ 0 & \dfrac{\Delta t}{R_u a_s} \end{bmatrix} \tag{19}$$

Equation (16) is rewritten using parameters $A_d$ and $B_d$ as follows,

$$\begin{bmatrix} z_{1,k+1} \\ z_{2,k+1} \end{bmatrix} = A_d \begin{bmatrix} z_{1,k} \\ z_{2,k} \end{bmatrix} + B_d \begin{bmatrix} u_{q,1,k} \\ u_{q,2,k} \end{bmatrix} \tag{20}$$

where, $T_c$ and $T_s$ are represented by $z_1$ and $z_2$. $Q_{gen}$ and $T_e$ are represented by $u_{q,1}$ and $u_{q,2}$. The coefficients are defined as follows:

$$A_d = \begin{bmatrix} a_{11} & a_{12} \\ a_{21} & a_{22} \end{bmatrix}, \quad B_d = \begin{bmatrix} b_{11} & b_{12} \\ b_{21} & b_{22} \end{bmatrix}$$

Given the measurement data as $\{z_{1,i}\}_{i=0}^{N}, \{z_{2,i}\}_{i=0}^{N}, \{u_{q,1,i}\}_{i=0}^{N}$ and $\{u_{q,2,i}\}_{i=0}^{N}$. Where, $N$ is the sampling number. Equation (20) can be rewritten as linear function as follows:

$$\hat{Z}(k) = \Phi^T(k)\Theta \tag{21}$$

where, $\hat{Z}(k)$ is the state estimation value and is satisfied as:

$$\hat{Z}(k) = \begin{bmatrix} \hat{z}_{1,1} & \hat{z}_{2,1} \\ \hat{z}_{1,2} & \hat{z}_{2,2} \\ \vdots & \vdots \\ \hat{z}_{1,k} & \hat{z}_{2,k} \end{bmatrix}$$

$$\Phi^T(k)=\begin{bmatrix} z_{1,0} & z_{2,0} & u_{q,1,0} & u_{q,2,0} \\ z_{1,1} & z_{2,1} & u_{q,1,1} & u_{q,2,1} \\ \vdots & \vdots & \ddots & \vdots \\ z_{1,k-1} & z_{2,k-1} & u_{q,1,k-1} & u_{q,2,k-1} \end{bmatrix}$$

$$\Theta=\begin{bmatrix} A_d & B_d \end{bmatrix}^T \tag{22}$$

By minimising the different value between the measured results and the estimated results, the parameters can be calculated. The optimisation objective function is shown as equation (23),

$$F_{opt}(k)=\frac{1}{N}\sum_{k=1}^{N}\left\|Z(k)-\Phi^T(k)\Theta\right\|_2 \tag{23}$$

The parameter identification results can be obtained using function (24),

$$\Theta^*=\arg\min F_{opt}(k) \tag{24}$$

## 4 Thermal fault diagnosis method

The flow chart of fault information diagnosis is shown in Figure 3. Observer 1 is designed to estimate battery internal resistance based on Lyapunov observer. Observer 2 is designed to estimate the core temperature based on extended Kalman filter. The inputs of Observer 1 are load current $I_{L_t}$ and terminal voltage $U_t$. The outputs of Observer 1 are the estimated value defined as $\hat{R}_{dc}$, $\hat{R}_o$ and $\hat{U}_{oc}$. The inputs of Observer 2 are surface temperature $T_s$ and the core temperature $T_c$. The outputs Observer 2 are the estimated value defined as $\hat{T}_s$ and $\hat{T}_c$. The differential equations of temperatures $T_s$ and $T_c$ are shown as equations (25) and (26),

$$\dot{T}_c=-\frac{T_c}{R_c a_c}+\frac{T_s}{R_c a_c}-\frac{I_L(U_t-U_{oc})}{a_c} \tag{25}$$

$$\dot{T}_s=-T_s\left(\frac{1}{R_c a_s}+\frac{1}{R_u a_s}\right)+\frac{T_c}{R_c a_s}+\frac{T_e}{R_u a_s} \tag{26}$$

To detect battery internal faults accurately and reliably, it is necessary to distinguish the system residual value in normal state and in fault state (Wu et al., 2017; Wang et al., 2017). The system residual error can be calculated as,

$$r_k=\left[\hat{z}_{1,k}+\frac{\hat{R}_{dc}}{\partial g/\partial z_1\big|_{z_1=\hat{z}_{1,k}}};T\right]-\left[\hat{z}_{1,k},\hat{z}_{2,k}\right] \tag{27}$$

where, $g$ is the relationship function of $R_{dc}$ and $T_c$. $r_k$ is a white Gaussian process in normal state and its mean value is considered as zero. However, the mean value of $r_k$ is

non-zero when the system is in fault state. Based on the state space equation of core temperature and surface temperature, the fault model can be written as follows,

$$z_{k+1} = A_d z_k + B_d u_{q,k} + f_k + \eta_k \tag{28}$$

where, $f_k \triangleq [f_1, f_2]^T$ are the fault vectors. The residual error $\dot{z}_1$ will be greater than the threshold value when the battery is on the condition of overcharge/over-discharge or short circuit( $f_k$ is defined as $f_1 \neq 0$ and $f_2 = 0$ ). The residual error $\dot{z}_2$ will be greater than the threshold value when the cooling system fails ( $f_k$ is defined as $f_1 = 0$ and $f_2 \neq 0$ ). When the internal resistance fails, $\dot{z}_1$ and $\dot{z}_2$ are both greater than the threshold value ( $f_k$ is defined as $f_1 \neq 0$ and $f_2 \neq 0$ ).

**Figure 3** Flow chart of fault information diagnosis (see online version for colours)

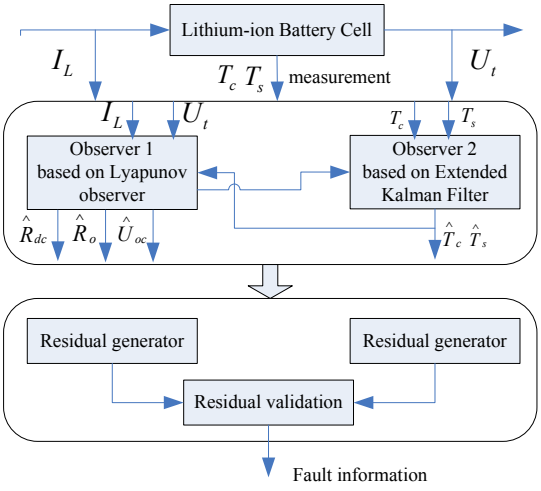


Given the residual error samples defined as $r_{k-s+1}, r_{k-s+2}, \cdots, r_k$ . Where, $s$ is the nearest sample number. The thermal fault diagnosis can be described as follows,

$$\left|\bar{r}_k\right| \leq \kappa_{th} : no\ fault$$

$$\left|\bar{r}_k\right| > \kappa_{th} : fault \tag{29}$$

where, $\bar{r}_k = \sum_{j=k-s+1}^{k} r_j / s$ . $\kappa_{th}$ is the fault threshold. Because the system parameters are uncertainty and the system models are inaccuracy, the fault threshold must be determined adaptively. The system uncertainty is expressed as $W \triangleq [w_1, w_2]^T$ . The thermal model can be rewritten as follows,

$$z_k = A_d z_{k-1} + B_d u_{q,k} + W \tag{30}$$

where, $W \in R^{2\times 1}$ . The fault can be decoupled from the system input vectors using the linear state transition matrix. The uncertainty of the thermal model is mainly caused by

the parameters of $a_c$, $a_s$, $R_{dc}$ and $T_e$. Therefore, the system uncertainty can be expressed as follows,

$$w_1 = p_{11}z_1 + p_{12}z_2 + p_{13}Q_{gen} + p_{14} \tag{31}$$

$$w_2 = p_{21}z_1 + p_{22}z_2 + p_{23}T_e + p_{24} \tag{32}$$

where, $p$ is the boundary coefficient. Based on the Kalman filtering algorithm, the residual error can be expressed as follows,

$$\dot{z}_k = \underbrace{(A_d - L_k C_d)}_{A_{e,k}} \dot{z}_{k-1} + W \tag{33}$$

Considering equations (18) and (19), the solution of equation (33) can be expressed as follows,

$$\dot{z}_k = \prod_{j=1}^{k} A_{e,j}\, \dot{z}_0 + [\sum_{i=1}^{k-1} (\prod_{j=i+1}^{k} A_{e,j}) + I] \bullet W \tag{34}$$

Based on inequality defined as $ab \le |ab| \le |a||b|$, the equation (34) can be rewritten as follows,

$$\dot{z}_k \le \prod_{j=1}^{k} A_{e,j} \left|\dot{z}_0\right| + [\sum_{i=1}^{k-1} (\prod_{j=i+1}^{k} A_{e,j}) + I] \bullet W \tag{35}$$

Combining equations (30)–(32), $W$ can be further written as follows,

$$|w_1| \le w_{1,b} \overset{\Delta}{=} p_{11,b}|z_1| + p_{12,b}|z_2| + p_{13,b}|Q_{gen}| + p_{14,b} \tag{36}$$

$$|w_2| \le w_{2,b} \overset{\Delta}{=} p_{21,b}|z_1| + p_{22,b}|z_2| + p_{23,b}|T_e| + p_{24,b} \tag{37}$$

where, $W_b = \left[w_{1,b}, w_{2,b}\right]^T$ represents the limit of model uncertainty. Function (35) can be rewritten as,

$$\dot{z}_k \le \kappa_k = \prod_{j=1}^{k} A_{e,j} \left|\dot{z}_k\right| + [\sum_{i=1}^{k-1} (\prod_{j=i+1}^{k} A_{e,j}) + I] \bullet W_b \tag{38}$$

where, $\kappa_1$ and $\kappa_2$ are the state threshold vectors defined as function (29). The second item on the right side of equation (38) can be equivalent as follows,

$$\zeta_k = A_{e,k}\zeta_{k-1} + W_b \tag{39}$$

where, the adaptive state threshold is defined as $\zeta = [\kappa_1, \kappa_2]^T$. The system residual threshold can be calculated using equation (40),

$$\kappa_k = \prod_{j=1}^{k} A_{e,j} \left|\bar{z}_0\right| + \zeta_k \tag{40}$$

The derivation process and analysis above indicate that the different thermal faults can be expressed by the system residual.

## 5 Experimental results and its analysis

### *5.1 Verification of thermal model parameters*

The UDDS dynamic working condition is used to verify our coupled electrothermal model (Wang et al., 2017). The test data of terminal voltage is shown in Figure 4. The first 1500 sampling data are used to calculate the model parameters. Based on equations (21)–(24), the system matrix is calculated based on Observer 1 as follows:

$$A_d = \begin{bmatrix} 0.8948 & 0.0153 \\ 0.0364 & 0.8567 \end{bmatrix}, \; B_d = \begin{bmatrix} 0.013 & 0 \\ 0 & 0.021 \end{bmatrix}$$

The estimated results and the measured value of $T_c$ and $T_s$ with the calculated $A_d$ and $B_d$ are shown in Figure 5. The estimation error (MAE) and the root mean square error (RMSE) are shown in Table 1. We also use the extended Kalman filtering algorithm to calculate the parameters. As shown in Figure 5, the estimation curve of $T_c$ converges to the measurement curve. The estimation error of $T_s$ is greater than $T_c$. During the initial sampling time within 500 s, the maximum estimation error of $T_s$ is 0.88°C. Based on Observer 1, the RMSE of $T_c$ and $T_s$ are 0.13°C and 0.25°C, respectively. The MAE is 0.49°C and 0.89°C, respectively. However, the RMSE and MAE value could be greater based on $A_d$ and $B_d$ using EKF.

**Table 1** Estimation error and RMSE of $T_c$ and $T_s$ based on observer 1 and EKF

| | *Observer 1* | | | | | | | | *EKF* | | | |
|---|---|---|---|---|---|---|---|---|---|---|---|---|
| *Estimation error*(°C) | *Temperature maximum absolute error* (°C) | | | | | | | | *Root mean square error* (°C) | | *Maximum absolute error* (°C) | *Root mean square error*(°C) |
| Sampling time(s) | 50 | 200 | 500 | 100 | 1500 | 2000 | 2500 | 3000 | | | | |
| $T_c$ | 0.08 | –0.05 | –0.20 | 0.28 | 0.49 | 0.16 | 0.12 | 0.30 | 0.49 | 0.13 | 0.57 | 0.25 |
| $T_s$ | –0.68 | –0.55 | –0.088 | 0.50 | –0.22 | –0.80 | 0.75 | 0.87 | 0.88 | 0.27 | 0.96 | 0.38 |

**Figure 4** The test data of terminal voltage (see online version for colours)

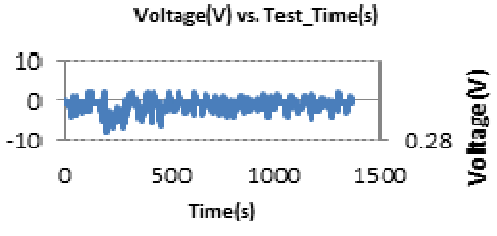

**Figure 5** Estimated and measured results of $T_c$ and $T_s$ based on $A_d / B_d$ value and observer 1 (see online version for colours)

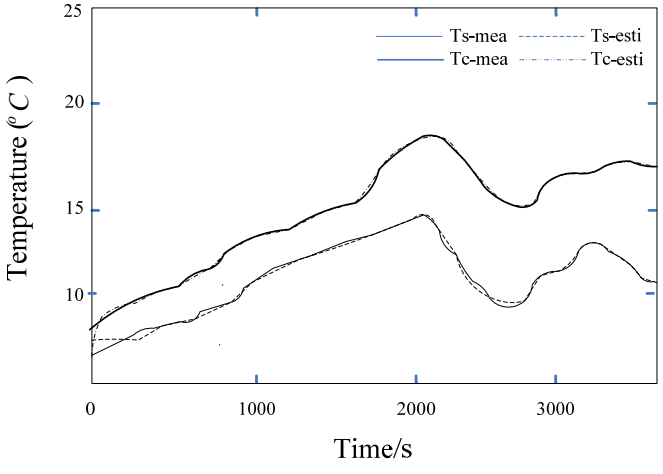


## *5.2 Verification of fault diagnosis methods*

Based on equations (18) and (19), the other parameters can be calculated as follows: $R_c = 2.64^o C/W$, $R_u = 3.49^o C/W$, $a_c = 68.4J/^{\circ}\text{C}$, $a_s = 14.3J/^{\circ}\text{C}$. In order to determine the model boundary value, the part of the model parameters are allowed to be disturbed (10%). The boundary condition parameters could be defined as $p_{11} = p_{22} = 10^{-5}$, $p_{12} = p_{21} = 10^{-4}$, $p_{13} = p_{14} = p_{24} = 0$ and $p_{23} = 10^{-4}$. The thermal diagnosis results without thermal fault are shown in Figure 6. The residual signals of $T_c$ and $T_s$ are given in Figure 6(a) and (b), respectively. The range surrounded by the upper and lower solid lines is the fault free safety range. The results indicate that both signals are close to zero. The different value of $r_1$ and $r_2$ determines the residual signals of temperature value. As shown in Figure 6, the boundary value of $r_1$ is ranged within $\pm 0.02^{\circ}\text{C}$ and the boundary value of $r_2$ is within $\pm 0.01^{\circ}\text{C}$. The parameter $\kappa$ represents the dynamic change of parameter $\zeta$. The residual signals of $T_c$ is within boundary value based on $\kappa_1$. The residual signals of $T_s$ is deviated based on $\kappa_2$.

To verify our proposed fault diagnosis method, $Q_{gen}$ is inserted from sample time of 1000 second. The residual signals of $T_c$ and $T_s$ are given in Figure 7(a) and (b), respectively. When the residual errors of $r_1$ is 0.12 W, the residual signals of $T_c$ is close to zero. The value is deviated to boundary curve when $r_1$ is 0.2 W. As shown in Figure 7, the residual signals of $T_s$ are close to zero when $r_2$ are both equal to 0.12W and 0.2W. Meanwhile, the minimum diagnosable thermal value is 0.12 W and the average thermal value is about 1.97 W after 1000 s.

**Figure 6** Simulation results of $T_c$ and $T_s$ without thermal fault: (a) residual signal of $T_c$ and (b) residual signal of $T_s$ (see online version for colours)

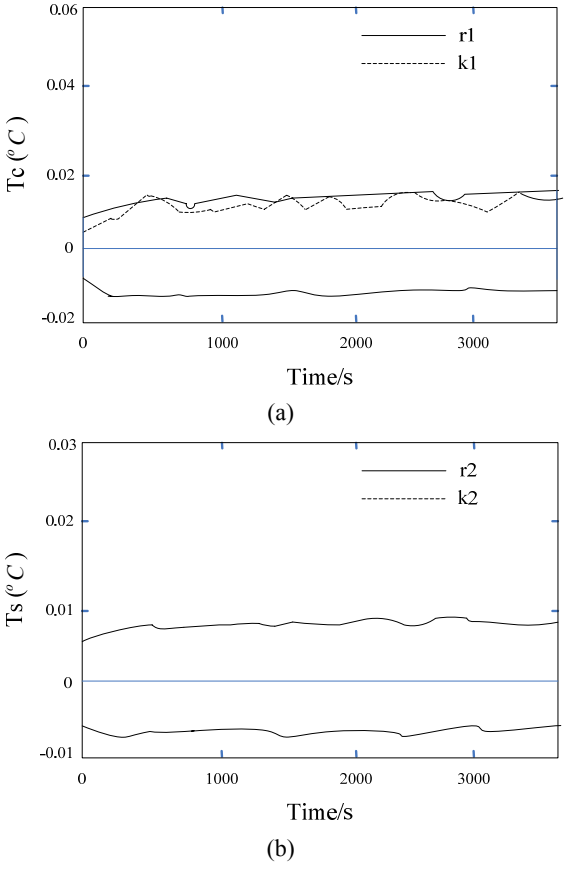


**Figure 7** Simulation results of $T_c$ and $T_s$ with thermal fault: (a) residual signal of $T_c$ and (b) residual signal of $T_s$ (see online version for colours)

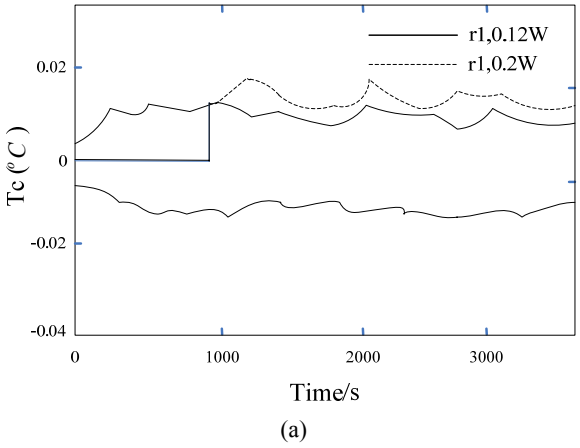

**Figure 7** Simulation results of $T_c$ and $T_s$ with thermal fault: (a) residual signal of $T_c$ and (b) residual signal of $T_s$ (see online version for colours) (continued)

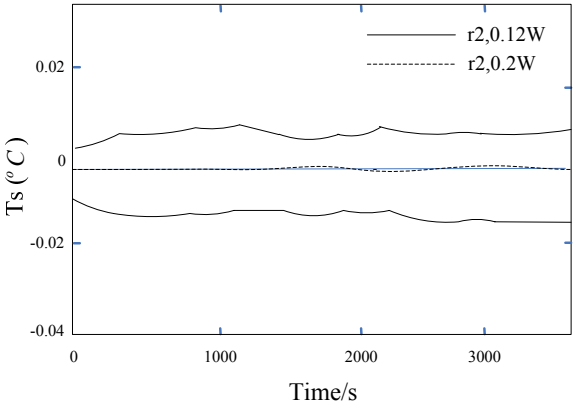


(b)

## 6 Conclusions

Thermal fault is one of the most critical failures during the battery working period. It must be diagnosed online and accurately. Firstly, the thermal generation mechanism of the lithium-ion battery is analysed. The core temperature is monitored and the thermal fault is detected. Secondly, the coupled electrothermal model is established combining with the equivalent circuit model and the thermal model. The model parameters identification algorithm is proposed. Thirdly, the estimation method of internal resistance based on Lyapunov observer is presented. The estimation method of core temperature and surface temperature based on extended Kalman filter is put forwarded. Lastly, the thermal fault diagnosis method and adaptive residual threshold design scheme are given. Further works include considering more fault factors and different working conditions.

## Acknowledgement

This paper is supported by Scientific Research Foundation of Hangzhou City University (No. J-202209 and No. X-202204). This work is supported by Edge Intelligence Technology and Equipment for Zhejiang Engineering Research Center.

## References

Chaou, I.H. and Ibe-Ekeocha, C.C. (2017) 'State of charge and state of health estimation for lithium-ion batteries using recurrent neural networks', *IEEE Transactions on Vehicular Technology*, Vol. 66, No. 10, pp.8773–8783.

Chen, J., Jiaqiang, E., Kang, S., Zhao, X., Zhu, H., Deng, Y., Peng, Q. and Zhang, Z. (2019) 'Modeling and characterization of the mass transfer and thermal mechanics of the power lithium manganate battery under charging process', *Energy*, Vol. 187, p.115924.

Dong, G.Z., Chen, Z.H., Wei, J.W. and Ling, Q. (2018) 'Battery health prognosis using Brownian motion modeling and particle filtering', *IEEE Transactions on Industrial Electronics*, Vol. 65, No. 11, pp.8646–8655.

Fan, G., Li, X. and Canova, M. (2018) 'A reduced-order electrochemical model of li-ion batteries for control and estimation applications', *IEEE Transactions on Vehicular Technology*, Vol. 67, No. 1, pp.76–91.

Fang, W., Kwon, O.J. and Wang, C.Y. (2010) 'Ectrochemical-thermal modeling of automotive Li-ion batteries and experimental validation using a three-electrode cell', *International Journal of Energy Research.*, Vol. 34, No. 2, pp.107–115.

Lam, A.Y., James, J. and Hou, Y. (2018) 'Coordinated autonomous vehicle parking for vehicles-to-grid services: formulation and distributed algorithm', *IEEE Transactions on Smart Grid*, Vol. 9, No. 5, pp.4356–4366.

Li, J., Wang, L.C. and Yu, L. (2017) 'State of charge estimation based on a simplified electrochemical model for a single licoo2 battery and battery pack', *Energy*, Vol. 133, pp.572–583.

Lian, J., Wang, X-r., Li, L-h., Zhou, Y-f., Yu, S-z. and Liu, X-j. (2020) 'Plug-in HEV energy management strategy based on SOC trajectory', *International Journal of Vehicle Design*, Vol. 82, No. 1, pp.1–17.

Liu, C., Wang, Y. and Chen, Z. (2019) 'Degradation model and cycle life prediction for lithium-ion battery used in hybrid energy storage system', *Energy*., Vol. 166, pp.796–806.

Liu, Z. and He, H. (2017) 'Sensor fault detection and isolation for a lithium-ion battery pack in electric vehicles using adaptive extended Kalman filter', *Applied Energy*., Vol. 185, pp.2033–2044.

Mangoni, D. and Soldati, A. (2021) 'Model-based simulation of dynamic behaviour of electric powertrains and their limitation induced by battery current saturation', *International Journal of Renewable Energy Technology*, Vol. 7, Nos. 1–2, pp.156–169.

Richardson, R.R., Birkl, C.R. and Osborne, E.M. (2018) 'Gaussian process regression for in-situ capacity estimation of lithium-ion batteries', *IEEE Transactions on Industrial Informatics.*, Vol. 99, pp.1–1.

Richardson, R.R., Osborne, M.A. and Howey, D.A. (2017) 'Gaussian process regression for forecasting battery state of health', *Journal of Power Sources.*, Vol. 357, pp.209–219.

Stoppanin, E. (2017) 'Smart charging and energy storage: bridging the gap between electromobility and electricity systems', *European Energy Journal*, Vol. 6, No. 4, pp.29–45.

Wang, Q., Jiang, B. and Li, B. (2016) 'A critical review of thermal management models and solutions of lithium-ion batteries for the development of pure electric vehicle', *Renewable and Sustainable Energy Reviews*., Vol. 64, pp.106–128.

Wang, Z., Hong, J. and Liu, P. (2017) 'Voltage fault diagnoses and prognosis of battery systems based on entropy and z-score for electric vehicles', *Applied Energy*., Vol. 196, pp.289–302.

Wu, C., Zhu, C. and Ge, Y. (2017) 'A new fault diagnosis and prognosis technology for high-power lithium-ion battery', *IEEE Transactions on Plasma Science*, Vol. 45, No. 7, pp.1533–1538.

Yang, S-c., Hua, Y., Qiao, D., Lian, Y-b., Pan, Y-w. and He, Y-l. (2019) 'A coupled electrochemical-thermal-mechanical degradation modelling approach for lifetime assessment of lithium-ion batteries', *Electrochimica Acta*, Vol. 326, pp.1–12.

Yassine, W. and Anderson, K.R. (2020) 'Testing and simulation of a solar PV/battery storage system with and without PWM charge control', *International Journal of Renewable Energy Technology*, Vol. 11, No. 1, pp.86–90.

Zhang, J., Li, X. and Liu, D. (2019) 'Mine car suspension parameter optimisation based on improved particle swarm optimisation and approximation model', *International Journal of Vehicle Design*, Vol. 80, No. 1, pp.23–40.

Zou, C., Hu, X. and Wei, Z. (2018) 'Electrochemical estimation and control for lithium-ion battery health-aware fast charging', *IEEE Transactions on Industrial Electronics*, Vol. 65, No. 8, pp.6635–6645.

## List of Symbols

| | |
|---|---|
| EKF | Extended Kalman filter |
| UDDS | Urban Dynamometer Driving Schedule |
| OCV | Open circuit voltage |
| $j$ | Positive pole |
| $\rho$ | Mass density of the battery |
| $c$ | Specific heat |
| $T$ | Battery temperature |
| $\lambda$ | Thermal conductivity |
| $I$ | Load current |
| $i_e(x,t)$ | Local current of electrolyte |
| $\Phi_s$, $\Phi_e$ | Electrode potential and electrolyte potential |
| $F$ | Faraday constant |
| $s$ | Cross-sectional area of solid particle surface |
| $J$ | Total ion flux on solid particle surface |
| $\Delta_s$ | Entropy change |
| $c_p$ | Specific thermal capacity |
| $V_b$ | Cell volume |
| $Q(t)$ | Thermal production |
| $r$ | Radial length |
| $t$ | Sample time |
| $R$ | Cell radius |
| $T_s$ | Surface temperature |
| $T_e$ | Environment temperature |
| $T_c$ | Core temperature |
| $h$ | Convection coefficient |
| $a_c$, $a_s$ | Heat capacity coefficients |
| $R_c$ | Thermal resistance |
| $R_u$ | Convection resistance |

| | |
|---|---|
| $Q_{gen}$ | Thermal production rate |
| $U_t$ | Terminal voltage |
| $U_{oc}$ | Open circuit voltage |
| $U_1$ | Cross voltage |
| $R_{dc}$ | DC internal resistance |
| $H$ | State transition matrix |
| $C$ | Battery observation matrix |
| $\eta_k$ , $v_k$ | Independent Gaussian noise |
| $A_d$ , $B_d$ | Coefficient matrix |
| $\hat{Z}(k)$ | State estimation value |
| $g$ | relationship function of $R_{dc}$ and $T_c$ |
| $\kappa_{th}$ | Fault threshold |
| $p$ | Boundary coefficient |
| $\kappa_1$ , $\kappa_2$ | State threshold vectors |